

Exposure Diffusion: HDR Image Generation by Consistent LDR denoising

MOJTABA BEMANA, MPI Informatik, Germany
 THOMAS LEIMKÜHLER, MPI Informatik, Germany
 KAROL MYSZKOWSKI, MPI Informatik, Germany
 HANS-PETER SEIDEL, MPI Informatik, Germany
 TOBIAS RITSCHHEL, University College London, United Kingdom



Fig. 1. Existing denoising diffusion models (top row) generate images with low-dynamic range (LDR) on a certain exposure, in the center. When re-exposed to other levels, bright parts like the lamps do not retain their contrast, and dark areas do not reveal details as in the shadow below the table. In our high-dynamic range (HDR) approach (bottom), diffusion is performed at multiple exposures, such that the lamps retain their contrast and the details in the animals’ bodies are produced without noise (see insets). An example application is an HDR display, where high pixel values map to high physical intensity.

We demonstrate generating high-dynamic range (HDR) images using the concerted action of multiple black-box, pre-trained low-dynamic range (LDR) image diffusion models. Common diffusion models are not HDR as, first, there is no sufficiently large HDR image dataset available to re-train them, and, second, even if it was, re-training such models is impossible for most compute budgets. Instead, we seek inspiration from the HDR image capture literature that traditionally fuses sets of LDR images, called “brackets”, to produce a single HDR image. We operate multiple denoising processes to generate multiple LDR brackets that together form a valid HDR result. To this end, we introduce an exposure consistency term into the diffusion process to couple the brackets such that they agree across the exposure range they share. We demonstrate HDR versions of state-of-the-art unconditional and conditional as well as restoration-type (LDR2HDR) generative modeling.

CCS Concepts: • **Computing methodologies** → **Computer graphics**.

Additional Key Words and Phrases: Augmented Reality

1 INTRODUCTION

Images generated by modern denoising diffusion models [Rombach et al. 2022; Sohl-Dickstein et al. 2015] have shown an unprecedented combination of user control and image quality. Unfortunately, the resulting images are low-dynamic range (LDR) while in computer graphics, several applications, such as physically-based simulation

and rendering [Debevec 1998], scene reconstruction involving profound shadows and specular highlights [Huang et al. 2022; Jun-Seong et al. 2022; Mildenhall et al. 2022], as well as advanced displays [Seetzen et al. 2004] require high-dynamic range (HDR).

We propose to close this gap by introducing a simple and effective method to upgrade a black-box denoising diffusion model from LDR to HDR image generation.

This poses two main challenges: first, the *limited scale of the available HDR training data*, which is orders of magnitude lower than its HDR counterpart, and second, the fact that for most users, it is *impossible to re-train the denoiser due to the sheer compute requirements*. We overcome the first challenge by avoiding producing HDR directly. Instead, we produce a set of individual *brackets*, i.e., LDR images, which can be merged into an HDR image. This allows us to circumvent the first challenge by never operating the denoiser on HDR images, and hence, also overcome the second challenge, as we circumvent the need to re-train the denoiser in HDR. Our method does not need any fine-tuning or training and considers the denoiser a black box.

Instead, the task is to produce brackets that are meaningful, i.e., meaningful on their own and meaningful in combination with other brackets (Fig. 2). To be plausible on its own, a bracket should have all details, without noise, in the range of values it represents. To work as a combination, a value in one bracket must match its value re-exposed to another bracket and ultimately when they are merged. We achieve these properties by deriving a diffusion process based on

Authors’ addresses: Mojtaba Bemana, MPI Informatik, Germany, mbemana@mpi-inf.mpg.de; Thomas Leimkühler, MPI Informatik, Germany, thomas.leimkuehler@mpi-inf.mpg.de; Karol Myszkowski, MPI Informatik, Germany, karol@mpi-inf.mpg.de; Hans-Peter Seidel, MPI Informatik, Germany, hpseidel@mpi-sb.mpg.de; Tobias Ritschel, University College London, United Kingdom, t.ritschel@ucl.ac.uk.

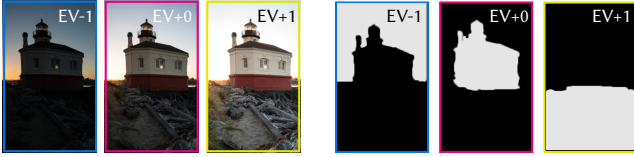


Fig. 2. Recalling HDR merging: LDR brackets are shown on the left; right, the weights for each bracket, for simplicity in binary. White means this pixel will contribute to the final HDR.

ideas from diffusion posterior sampling (DPS) [Chung et al. 2023] that operates between multiple brackets jointly.

2 BACKGROUND: MULTI-EXPOSURE HDR IMAGING

HDR images directly register scene radiance, typically up to a scale factor, so that image details in the darkest and brightest scene regions are readily available. As sensors with HDR capabilities are relatively rare and expensive, typically, a stack of differently exposed LDR photographs (refer to Fig. 2) is merged into an HDR image [Debevec and Malik 1997; Mitsunaga and Nayar 1999; Robertson et al. 2003; Wang et al. 2023b]. By transforming each pixel value through an inverted camera response and then dividing by the exposure time, a measurement of the scene radiance can be derived [Reinhard et al. 2010]. As such, per-pixel measurements are the most reliable in the middle range of the camera response [Debevec and Malik 1997]; an accordingly weighted average of the measurements can be computed for all exposures. Fig. 2-right shows a simplified version of such weights for exposures EV-1, EV+0, and EV+1, where EV+ x denotes multiplying with 2^x in the linear radiance space. Note that the radiance ranges below the black level and over 1 are covered just in a single exposure EV+1 and EV-1, respectively, while for EV+0, radiance information is clamped on both sides of the range. Dark image regions are also contaminated with sensor noise, whose characteristics may differ between exposures, which makes consistent denoising difficult [Chang et al. 2020; Cogalan et al. 2022; Mustaniemi et al. 2020]. Some camera manufacturers introduce hard clamping at a black-level radiance, assuming that there is no reliable image information below this threshold due to noise. Finally, the performance of the multi-exposure methods might be limited for large scene/camera motion that causes ghosting that is further aggravated by simultaneous image saturation [Kalantari and Ramamoorthi 2017; Wu et al. 2018; Yan et al. 2019, 2020]. The latter problem can be reduced through consistent image hallucination using adversarial training [Li et al. 2022; Niu et al. 2021] or conditional diffusion [Yan et al. 2023] components.

In this work, we aim to use diffusion [Chung et al. 2023; Ho et al. 2020; Sohl-Dickstein et al. 2015] to generate consistent multiple exposures. In this process, we need to account for missing information due to clamping and, when relevant, denoise.

3 PREVIOUS WORK

In this section, we discuss previous work on deep single-image HDR reconstruction methods and the use of diffusion models in HDR imaging that are central to this work. A broader perspective on

other aspects of deep learning for HDR imaging can be found in a recent survey [Wang and Yoon 2022].

Deep single-image HDR reconstruction (LDR2HDR). An alternative solution to multi-exposure techniques (Sec. 2) relies on restoring HDR information from a single LDR image. Traditional methods are extensively covered in Banterle et al. [2017], and here, we focus on recent machine-learning solutions. Single-image HDR reconstruction can be performed directly [Chen et al. 2022; Eilertsen et al. 2017; Liu et al. 2020; Marnerides et al. 2018; Santos et al. 2020; Yu et al. 2021; Zhang and Aydin 2021], or, alternatively, by first producing a stack of different exposures that are then merged into an HDR image [Endo et al. 2017; Jo et al. 2021; Lee et al. 2018a,b, 2020]. Specialized solutions are required when an observation EV+0 is captured in dark conditions, where denoising is a key problem [Chen et al. 2018; Wang et al. 2023c]. Text conditioning driven by a contrastive language-image pre-training (CLIP) model [Radford et al. 2021] can be used for the generation of a well-exposed LDR environment map that is then transformed into its HDR counterpart by a fully supervised network [Chen et al. 2022]. Even though some methods employ adversarial training [Lee et al. 2018b; Zhang and Aydin 2021], the key problem remains limited performance in reconstructing clamped regions. Those methods mostly require LDR and HDR image pairs for training, which is problematic due to limited datasets. Recently, GlowGAN [Wang et al. 2023a] addressed the latter two problems by fully unsupervised learning a generative model of HDR images exclusively from in-the-wild LDR images. As this approach is based on StyleGAN-XL [Sauer et al. 2022], it requires GAN training on narrow domains (e.g., lightning, fireworks) to capture the respective HDR image distribution.

Diffusion models in HDR imaging. Denoising diffusion probabilistic models (DDPMs) [Ho et al. 2020; Sohl-Dickstein et al. 2015] demonstrate huge capacity in modeling complex distributions and typically outperform other generative models in terms of image realism, diversity, and detail reproduction [Dhariwal and Nichol 2021]. DDPMs also proved useful for solving linear [Song et al. 2021] and non-linear [Chung et al. 2023] inverse imaging problems that are common in image restoration and enhancement tasks guided by the degraded input image. Image inpainting [Lugmayr et al. 2022], deblurring [Kawar et al. 2022], and super-resolution [Saharia et al. 2023] are examples of such restoration tasks, where the degradation models are typically linear and known [Fei et al. 2023]. In HDR imaging tasks, the degradation model is more complex, and existing solutions based on DDPMs are more sparse. Wang et al. [2023c] propose low-light image enhancement using exposure diffusion that is directly initialized with the noisy low-light image instead of Gaussian noise, which greatly simplifies denoising and consequently reduces the network complexity and the required number of inference steps. The method can be trained using pairs of low-light and normally-exposed photographs, as well as synthetic data using different noise models. Fei et al. [2023] employ a pre-trained DDPM and propose the Generative Diffusion Prior (GDP) for unsupervised modeling of the natural image posterior distribution. They demonstrate the utility of this framework for low-light image enhancement and HDR image reconstruction by merging low, medium, and high exposures. A similar task, but with explicit emphasis on large motion

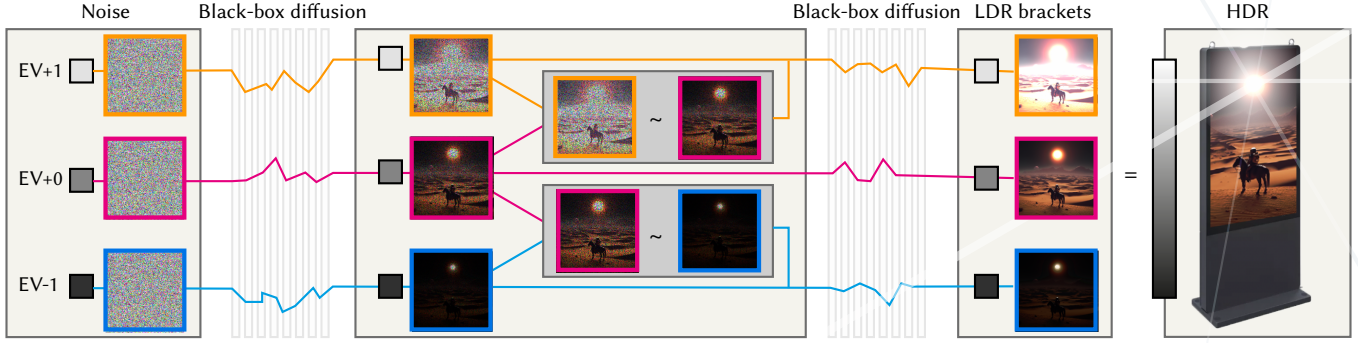


Fig. 3. Overview of our approach. Diffusion occurs from left to right and across multiple exposure levels (brackets), shown vertically. We show an example with three brackets. The process starts with three independent noises. At each diffusion step (one is shown), denoising is guided by an exposure consistency term (middle block). In this term, brackets are made consistent when re-exposed (\approx symbol). When diffusion has finished, the brackets form an HDR image under a common HDR fusion.

between the three exposures and severe clamping at the same time, is addressed in Yan et al. [2023]. Lyu et al. [2023] train a DDPM to capture the distribution of natural HDR environment maps, but are limited to rather narrow classes (e.g., urban streets) due to scarcity of available HDR training data. Dalal et al. [2023] train a DDPM on LDR–HDR image pairs (roughly 2,000 images, from the HDR-Real [Liu et al. 2020] and HDR-Eye [Nemoto et al. 2015] datasets) and reconstruct HDR images from single LDR images.

Our work follows [Chung et al. 2023] and relies on off-the-shelf pre-trained diffusion models [Dhariwal and Nichol 2021; Nichol et al. 2022] that feature better domain generalizability due to intensive training on large datasets than explicit training on small datasets of LDR–HDR image pairs [Dalal et al. 2023; Lyu et al. 2023]. Our solution does not require any HDR images at the training stage. Instead, we implicitly leverage the exposure statistics of real-world photographs used for DDPM training, which allows the model to reason on the underlying radiance distributions. In single-image reconstruction, we require as the input just one LDR exposure and then generate a stack of different spatially consistent LDR exposures. This way, we avoid possible problems with large motion inherent for time-sequential capturing [Fei et al. 2023; Yan et al. 2023].

Optionally, the hallucinated HDR content in saturated regions can be conditioned on text prompts [Nichol et al. 2022]. Such text prompts can also be used as the only input to generate standalone HDR images. Histograms with the desired pixel color distribution, possibly derived from existing images, can guide global contrast relations in generated HDR content and can optionally be combined with text prompts. Tab. 1 summarizes all text conditioning and image/histogram guidance combinations we support. With respect to non-diffusion methods such as GlowGAN [Wang et al. 2023a], we benefit from an overall better quality of generated images by diffusion models [Dhariwal and Nichol 2021; Nichol et al. 2022] and avoid a lossy inversion of an input LDR exposure into a latent code as required by GANs.

4 OUR APPROACH

We will first briefly recall the mechanics of sample generation using DDPMs with a guiding term (Sec. 4.1), before presenting our idea (Sec. 4.2).

4.1 Guided Diffusion

Data generation with a pre-trained DDPM [Ho et al. 2020; Sohl-Dickstein et al. 2015] amounts to gradual denoising of a sample $\mathbf{x} \in \mathbb{R}^u$ using

$$\mathbf{x}_{t-1} := \frac{1}{\sqrt{\alpha_t}} \left(\mathbf{x}_t - (1 - \alpha_t) \nabla_{\mathbf{x}_t} \log p_t(\mathbf{x}_t) \right) + \mathbf{z}_t. \quad (1)$$

This update rule involves a noise schedule $\alpha_t \in \mathbb{R}_+$, random vectors $\mathbf{z}_t \in \mathbb{R}^u$, and, at its core, a score function $\nabla_{\mathbf{x}_t} \log p_t(\mathbf{x}_t)$. Optionally, the score can be conditioned on a signal $\mathbf{c} \in \mathbb{R}^v$, such as a text prompt embedding, to yield $\nabla_{\mathbf{x}_t} \log p_t(\mathbf{x}_t | \mathbf{c})$. In modern DDPMs, scores are typically approximated by a neural network $\mathbf{s}_\theta(\mathbf{x}_t, \mathbf{c}, t) \in (\mathbb{R}^u \times \mathbb{R}^v \times \mathbb{Z}) \rightarrow \mathbb{R}^u$. Please refer to Yang et al. [2023] for an in-depth treatise.

In the framework of diffusion posterior sampling (DPS) [Chung et al. 2023], an additional guiding signal $\mathbf{y} \in \mathbb{R}^w$, such as a partial observation of \mathbf{x} , is incorporated into the denoising process to arrive at the posterior score

$$\nabla_{\mathbf{x}_t} \log p_t(\mathbf{x}_t | \mathbf{c}, \mathbf{y}) \approx \mathbf{s}_\theta(\mathbf{x}_t, \mathbf{c}, t) - \lambda \nabla_{\mathbf{x}_t} C(\hat{\mathbf{x}}_t, \mathbf{y}). \quad (2)$$

Here, $C \in (\mathbb{R}^u \times \mathbb{R}^w) \rightarrow \mathbb{R}$ is a problem-specific measurement term that drives the denoising process towards solutions that incorporate the guiding signal \mathbf{y} , and $\lambda \in \mathbb{R}_+$ is a balancing term. For increased stability, Chung et al. [2023] propose to feed the current estimate of the clean sample

$$\hat{\mathbf{x}}_t = \frac{1}{\sqrt{\bar{\alpha}_t}} \left(\mathbf{x}_t + (1 - \bar{\alpha}_t) \mathbf{s}_\theta(\mathbf{x}_t, \mathbf{c}, t) \right) \quad (3)$$

to C , where $\bar{\alpha}_t$ is derived from α_t .

4.2 Exposure diffusion

The above equations Eq. 1 and Eq. 2 are valid for producing a single LDR result image \mathbf{x} . Our idea is to produce HDR by diffusing multiple LDR results. Hence, we operate (Fig. 3) on a set of LDR images $\{\mathbf{x}^{-m}, \dots, \mathbf{x}^0, \dots, \mathbf{x}^n\}$, called “brackets”. Positive and negative superscripts denotes positive and negative EVs, respectively. All brackets are initialized to noise with mean zero and standard deviation one. They, further, need to be gamma-corrected sRGB LDR images, as we consider the score function a black box that cannot be retrained to work on linear HDR.

Score term. The first term in Eq. 2 is the common score function that points from the current solution into the direction of a more plausible one. It may or may not be conditioned as per the second column of Tab. 1, leading to different application scenarios.

It is a black box we do not need to know any details of, nor differentiate, as it already encodes a gradient. We only need to know its noise schedule α_t to also use \hat{x} from Eq. 3. The score function is hence simply computed on each bracket independently.

Posterior term. The second term in Eq. 2 is very specific to our problem, the exposure consistency cost term. The consistency of two brackets measures how much \hat{x}^i , a free variable, is compatible with another bracket \hat{x}^r that is assumed fixed. For each bracket \hat{x}^i , the reference bracket \hat{x}^r is exposed to another bracket, and the resulting differences are checked using a function *exco* (to be defined in the next paragraph).

The posterior term is slightly different for positive, negative and zero EV brackets:

$$C(\hat{x}^i, y) = \begin{cases} C_{\downarrow}(\hat{x}^i, \hat{x}^{i+1}) & , \text{if } i < 0, \text{ see Eq. 5,} \\ C_{\uparrow}(\hat{x}^i, \hat{x}^{i-1}) & , \text{if } i > 0, \text{ see Eq. 6 and} \\ C_0(\hat{x}^i, y) & , \text{if } i = 0, \text{ see Eq. 7.} \end{cases} \quad (4)$$

Both positive and negative posterior make use of two mask functions *sat* and *dark* which are one for saturated and near-zero pixels, respectively, and zero otherwise. In practice, we use smooth versions of that for better differentiability; a very smooth function $\text{sat}(x) = x$ and $\text{dark}(x) = 1 - x$ provides the best results.

The posterior for decreasing exposure is

$$C_{\downarrow}(\hat{x}^i, \hat{x}^r) = \|\text{sat}(\hat{x}^r) \cdot \max(\text{exco}(\hat{x}^r \rightarrow \hat{x}^i), 0)\|_2 + \lambda_s \cdot \|(1 - \text{sat}(\hat{x}^r)) \cdot (\text{exco}(\hat{x}^r \rightarrow \hat{x}^i))\|_2, \quad (5)$$

while the one to increase exposure is

$$C_{\uparrow}(\hat{x}^i, \hat{x}^r) = \|\text{dark}(\hat{x}^r) \cdot (\text{exco}(\hat{x}^r \rightarrow \hat{x}^i))\|_2 + \lambda_d \cdot \|(1 - \text{dark}(\hat{x}^r)) \cdot (\text{exco}(\hat{x}^r \rightarrow \hat{x}^i))\|_2, \quad (6)$$

where λ_s and λ_d are set to 1 and 2, respectively. Note that in Eq. 6, the two terms are weighted differently. This is because the darker regions *dark*(\hat{x}^r) are usually noisy or unreliable; thus, we impose less exposure consistency prior on these regions compared to the brighter regions. The exposure consistency *exco* of one LDR bracket \hat{x}^i with respect to a reference \hat{x}^r (that can both be higher or lower EV) is defined as

$$\text{exco}(\hat{x}^r \rightarrow \hat{x}^i) := \left(\min\left(\left(\frac{\beta^i}{\beta^r} \odot (\hat{x}^r)^{-\gamma}\right), 1\right) \right)^{\gamma} - \hat{x}^i,$$

where β stands for exposure time. We first undo the gamma ($\gamma = 2.2$), as the solution has to live in non-linear space for the black box score. Next, we scale by the ratio between the exposure times and then clamp and apply gamma again, as a real camera would. The result has returned to the domain an LDR score function can handle and is compared to the bracket \hat{x}^i in question.

The possible combinations of consistency and up or down direction are discussed for an example in Fig. 4.

Eq. 4 is the expression for a single exposure bracket \hat{x}^i . As per Eq. 2, this expression gets differentiated with respect to its first

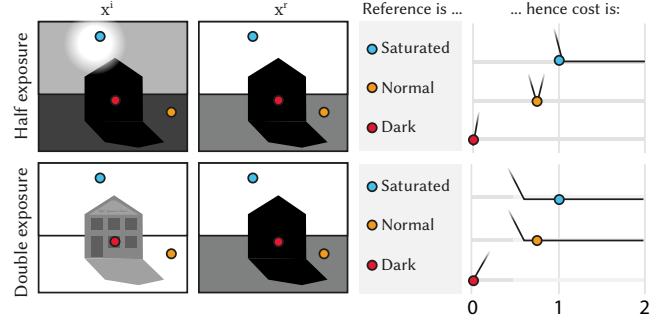


Fig. 4. Posterior based on exposure consistency cost for three representative points (colored dots) in two conditions (rows) when adjusting the current solution \hat{x}^i with respect to a reference bracket \hat{x}^r (columns). The top row goes down in exposure, bottom row goes up. The condition with respect to *dark* and *sat* is different for each representative point. Depending on the exposure direction, this results in different costs for choices in \hat{x}^i . In the cost plot, dots are placed horizontally where their value in the reference is.

Table 1. Different combinations of score conditioning, guidance, and whether including EV+0 in the posterior leads to different applications.

Application	Cond. c	Guide y	EV+0 fix?	Example
Generation	Text	—	×	Fig. 5
Generation	—	Histo.	×	Fig. 6
Generation	Text	Histo.	×	Fig. 7
Reconstruction	—	Image	✓	Fig. 10, 11, 12
Reconstruction	Text	Image	✓	Fig. 8

argument. The subtlety is that this is now done for multiple brackets, but they depend on each other. In our implementation, during one optimization step, however, for each bracket, the other bracket \hat{x}^r is considered a constant, so the second argument of C_{\downarrow} , C_{\uparrow} , and C_0 is “detached” in PyTorch parlance. Note that this is different from greedily optimizing each bracket sequentially.

Finally, we can also define an optional posterior term on the original image by applying a function f :

$$C_0(\hat{x}^i, y) = \lambda_c \cdot \|f(\hat{x}^i) - y\|_2. \quad (7)$$

First, if f is, for example, the identity, and y an LDR image (the third column in Tab. 1), this becomes a reconstruction task. In that case, the solution for \hat{x}^i is immediately set to y . As a second alternative, we explore using conversion to an LDR histogram as f . The parameter λ_c is always set to 10.

5 RESULTS

We demonstrate the application of our method to HDR generation (Sec. 5.2) and reconstruction (Sec. 5.3), demonstrating qualitative as well as quantitative results for both tasks.

5.1 Experimental setup

For our reconstruction experiments, specifically the LDR2HDR task, we utilize the pre-trained unconditional diffusion model [Dhariwal and Nichol 2021] directly without finetuning. Our input images

are down-sampled to 256×256 before they are fed to this model, and we perform 1,000 denoising steps to produce our results. In tasks involving text-conditioning or histogram guidance, we use the OpenAI GLIDE [Nichol et al. 2022] diffusion model, which is text-conditional and generates images at a resolution of 64×64 using a classifier-free guidance strategy. Subsequently, an upsampling diffusion model is applied to increase the resolution to 256×256 . In this case, we apply our DPS approach only to the text-conditional model. Once the exposure brackets are generated, they are individually upsampled with the upsampling module.

The hyper-parameter λ in Eq. 1 balances between the diffusion prior and our posterior term. In our experiments, a constant λ led to degenerated results; instead, we adopt λt^2 , gradually incorporating the posterior term with respect to the denoising step t . We set $\lambda = 3$ when using the unconditional diffusion model [Dhariwal and Nichol 2021] while opting for a lower value of $\lambda = 0.75$ when employing the conditional diffusion model [Nichol et al. 2022], as it operates on smaller image resolutions.

For all results, we compute five exposure brackets: EV-4, EV-2, EV+0, EV+2, and EV+4, unless otherwise specified. These exposure brackets are merged using the standard technique [Debevec and Malik 1997] to create our HDR image. For Fig. 11, Fig. 8 and Fig. 12, we show the result of applying Mantiuk et al. [2006]’s tonemapping while in all other results, we directly show the optimized brackets.

5.2 Generation

Image generation is a premiere ability of diffusion models, which we extend to HDR. Image generation without any conditioning or guidance frequently results in scenes that, in reality, do not exhibit high dynamic ranges. Therefore, capitalizing on the generality of our framework, we consider generation conditioned on text prompts, guided by RGB color histograms, and a combination thereof (first three rows in Tab. 1).

Text-based. Here, we consider the task of text-conditioned generation, where the score function takes a conditioning signal c in the form of a text embedding. We omit C_0 , i.e., the generation is free to synthesize any consistent brackets following the text prompt. Results of this application are shown in Fig. 5. The low exposures present detailed depictions of visible light sources, such as the structure of candle flames, including glares typically found around strong light sources. In the daylight scenes, most of the details are properly exposed for the medium exposure (EV+0), while in the night scenes, a high exposure (EV+4) is required to see sufficient detail.

Histogram-based. Here, we explore guided generation using a target histogram. In our experiments, we first compute an LDR histogram with 10 bins per color channel of an input image as our guiding signal y (Fig. 6, first column). Then, we utilize C_0 to direct the generation process towards producing an EV+0 bracket that matches this histogram (Fig. 6, third column), using a differentiable histogram function with soft bin assignments as f . Our framework produces consistent brackets of HDR content (Fig. 6, second to fourth column).

Text & histogram-based. In Fig. 7, we combine the control modalities of the previous two paragraphs. In the first three rows, we apply

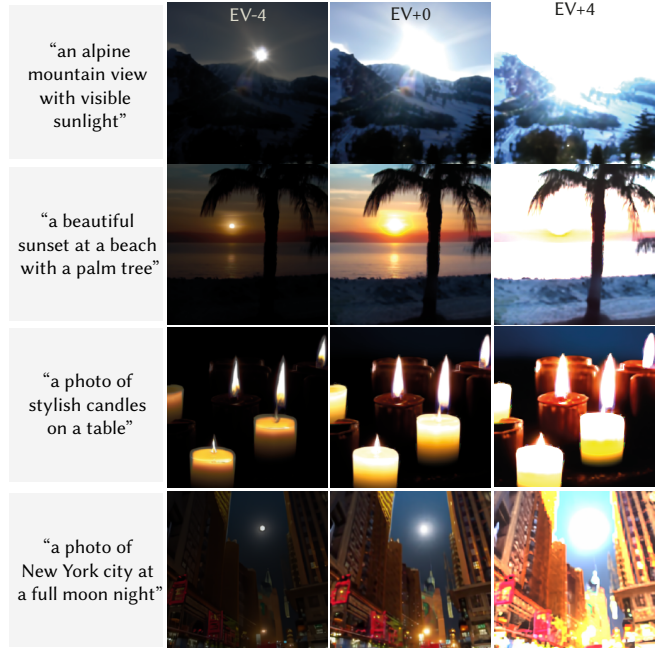


Fig. 5. Text-based HDR generation. Text prompts are on the left, alongside low (EV-4), medium (EV+0), and high exposures (EV+4). Please refer to our supplementary material for additional results.

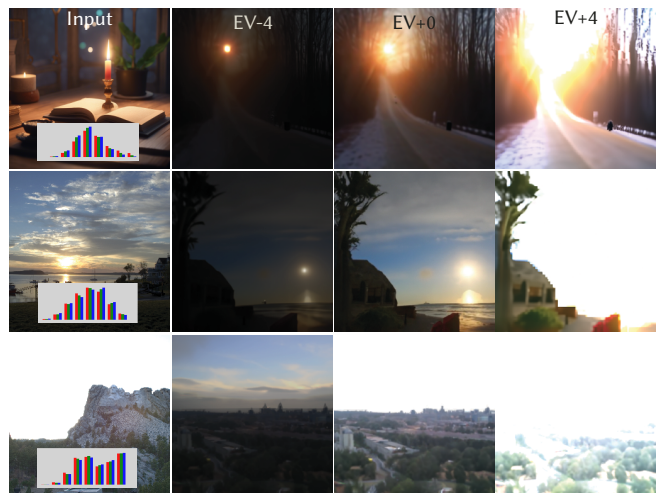


Fig. 6. Histogram-based HDR generation. The first column shows the input image and its histogram. The other columns show our generated brackets. Note that the method never sees the input image (left) only its histogram.

constraints where 50%, 25%, and 1% of saturated pixels are enforced on the histograms of the EV+0 bracket, all while utilizing the same text prompt. We observe that our approach enables the generation of different HDR contents that faithfully reflect the queries. In the last row, a guiding histogram is extracted from an input image.



Fig. 7. Text- and histogram-based HDR generation. The first column is the query, and the other three columns are our results.

Table 2. Reconstruction task performance.

Method	FID↓						No-Ref.↓	Full-Ref.↑
	EV-4	EV-2	EV+0	EV+2	EV+4	All.		
MaskHDR	14.36	09.44	04.13	01.14	02.81	<u>03.63</u>	51.7 ± 7.5	5.87 ± 1.6
HDRCNN	14.54	16.89	13.06	03.73	03.27	06.54	<u>47.2 ± 7.1</u>	6.67 ± 1.2
GlowGAN	<u>08.59</u>	<u>06.94</u>	05.32	03.61	08.09	03.08	45.5 ± 8.6	<u>6.57 ± 1.5</u>
Ours	06.25	06.48	<u>04.65</u>	<u>01.28</u>	<u>02.89</u>	02.05	51.7 ± 7.6	6.51 ± 1.2

5.3 Reconstruction

We now turn to one of the supreme disciplines of HDR imaging: LDR2HDR restoration. There are two major challenges involved in this task. Firstly, we need to fill the saturated (white) regions in the LDR image y with appropriate content. Secondly, dark regions in y often contain strong noise that needs to be removed. Our approach naturally supports this task by setting f in Eq. 7 to be the identity function. We demonstrate both unconditional and text-conditioned reconstruction (last two rows in Tab. 1).

Methods and dataset. We compare our unconditional approach against the three best-performing LDR2HDR methods according to a recent study [Wang et al. 2023a]: **MaskHDR** [Santos et al. 2020], **HDRCNN** [Eilertsen et al. 2017] and **GlowGAN** [Wang et al. 2023a]. Note that the only other generative approach, **GlowGAN**, requires training a domain-specific model. Thus, for a fair comparison, we limit our evaluation to landscape images, as a pre-trained **GlowGAN** model is available for this category. Specifically, we curate a dataset comprising 75 HDR images sourced from various online platforms, which will be made available on publication.

Metrics. We employ three different metrics to assess restoration performance. Firstly, we employ the full-reference metric HDR-VDP-3 [Mantiuk et al. 2023], which evaluates reconstruction fidelity without considering that saturated regions in an LDR image may allow for multiple, different HDR solutions. Secondly, to gauge overall plausibility, we utilize the no-reference HDR image metric PU21-PIQE [Hanji et al. 2022]. This metric, however, is agnostic of the expected distribution of hallucinated contents in our narrow domain.

To address these considerations, we further measure the FID score [Heusel et al. 2017], which is commonly used in generative settings for its ability to measure discrepancies between distributions. As this metric relies on a vision model [Krizhevsky et al. 2012] pre-trained on LDR images, we cannot directly feed HDR content into it. Rather, we seek to produce a representative distribution of LDR images derived from the HDR content, accounting for uncalibrated and unnormalized pixel values across methods. We opt to apply the auto-exposure method by Shim et al. [2014] to each HDR image. This technique helps determine the EV0 bracket, from which we derive EV±2 and EV±4 brackets. Subsequently, we select 100 random 64×64 -pixel crops from each image. We maintain consistency in selecting crop locations across methods [Chai et al. 2022]. This precaution is necessary because having small bright light sources, such as the sun, in some patches in one method but not in another, could disproportionately bias the measurement. Our protocol leads to stable estimates based on 7.5k patches per bracket and 37.5k patches in total.

Results. Our quantitative evaluation results are presented in Tab. 2. We observe that our approach outperforms the baselines in terms of aggregated FID and excels in the challenging cases of negative EV where content needs to be hallucinated. Results for the other two metrics remain inconclusive due to statistical insignificance.

In Fig. 11, we show corresponding qualitative results with a focus on saturated regions; complete sets of images are provided in the supplemental. Our approach consistently generates arguably the highest-quality hallucinations in saturated regions. This is facilitated by the first term in Eq. 5, which gives the process the freedom to generate any content, as long as it is bright enough. Notably, in the third row of Fig. 11, we present a particularly challenging case where one color channel is nearly entirely saturated across the image. In this instance, we observe how the baselines struggle to produce plausible content, even **GlowGAN**, which typically excels in generating realistic results due to its domain-specific generative capabilities. In the last two rows, we see that **HDRCNN** and **MaskCNN** struggle with image regions close to the sun, producing unnatural discontinuities and halo effects, respectively. As anticipated, given the inherent ambiguities of the LDR2HDR restoration task, all methods, including ours, generate results that diverge from the reference.

Another challenging aspect of LDR2HDR reconstruction involves eliminating noise from regions that were initially very dark. A naïve scaling of the original image content leads to substantial noise, making these results practically unusable. In Fig. 12, we illustrate how our approach serves as an effective denoiser, yielding visually pleasing outcomes.

Text-based reconstruction. Our framework offers a unique opportunity: the ability to dictate which content to hallucinate in saturated regions through text conditioning. This is demonstrated in Fig. 8, where, in addition to the guiding LDR signal y , the user provides a text prompt conditioning signal c . We see that this combination of control modalities enables precise HDR content generation. We emphasize that this task differs from typical inpainting in the LDR domain. Here, saturated pixel values are not replaced by darker ones, but rather extended in dynamic range while forced to align with the LDR observation (Eq. 5).

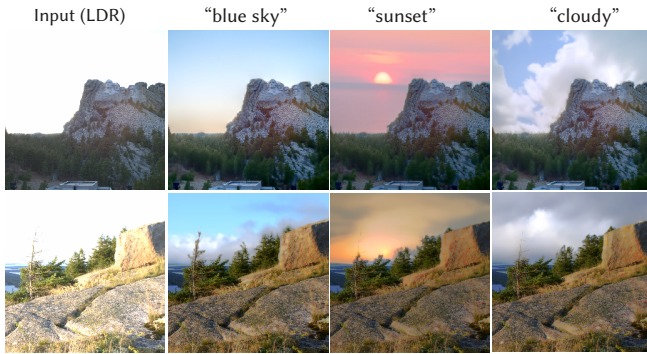


Fig. 8. Text-based reconstruction. The LDR image on the left has ambiguous regions, e.g., the sky. The right three columns show what the sky could look like in a tone-mapped result on a reconstructed HDR. Each variant is conditioned on different text prompts shown on the top.

Alternative solution. We further investigated the alternative choice of score distillation sampling (SDS) [Poole et al. 2022] for HDR generation. In this approach, we represent our HDR image using a 2D hash-grid neural network (NN) [Müller et al. 2022]. We choose to optimize an NN rather than a simple pixel grid as we observed the NN provides better results. During each optimization step, the HDR image is randomly exposed with $EV+x$, where x is drawn from a normal distribution with a mean of zero and a standard deviation of four. We compute the SDS loss on the exposed images and update the parameters of NN. The SDS loss guides the current estimate of the exposed images towards the manifold of natural images learned by the pre-trained diffusion model [Rombach et al. 2022]. In Fig. 9, we present our best-effort results. While this simpler approach can generate HDR content, achieving natural results remains challenging.

6 CONCLUSION

We have suggested a method to generate HDR images using a black-box diffusion-based image generation model. The key idea is to generate multiple LDR brackets in sync. The method is simple to implement, intuitive, and can produce results with unprecedented quality in bright lights and good noise removal in shadows. This is confirmed by the many results from our supplemental material and the results of baselines on these.

In future work, we would like to extend the presented ideas to other modalities involving multiple images, like multi-spectral, stereo, light fields, and combinations thereof. It would be interesting

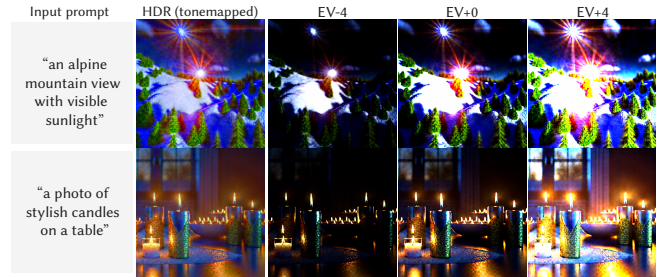


Fig. 9. HDR generation using SDS-based optimization [Poole et al. 2022]: the resulting images are HDR, but unfortunately not natural.



Fig. 10. Panoramic HDR generation at a 256×640 resolution given an AI-generated LDR image (middle row): To generate a panoramic image, we follow the diffusion composition technique from [Jiménez 2023] and simultaneously denoise three tiles of 256×256 resolution, each with a 64-pixel overlap, to ensure smooth transitions between them.

to adapt our DPS-based approach to stable/latent diffusion models [Rombach et al. 2022] and directly benefit from the higher image quality, as well as image resolution that they offer. Fine-tuning of large pre-trained diffusion models that require little paired training, such as ControlNet [Zhang et al. 2023] and Marigold [Ke et al. 2023], would be another interesting avenue of research. In this work, we have chosen to strictly avoid using any HDR images for training and mitigate possible issues due to limited image content classes that are available in existing HDR datasets.

REFERENCES

- Francesco Banterle, Alessandro Artusi, Kurt Debattista, and Alan Chalmers. 2017. *Advanced high dynamic range imaging*. AK Peters/CRC Press.
- Lucy Chai, Michael Gharbi, Eli Shechtman, Phillip Isola, and Richard Zhang. 2022. Any-resolution training for high-resolution image synthesis. In *ECCV*. 170–188.
- Meng Chang, Huajun Feng, Zhihai Xu, and Qi Li. 2020. Low-light Image Restoration with Short- and Long-exposure Raw Pairs. arXiv:2007.00199 [eess.IV]
- Chen Chen, Qifeng Chen, Jia Xu, and Vladlen Koltun. 2018. Learning to See in the Dark. In *CVPR*.
- Zhaoxi Chen, Guangcong Wang, and Ziwei Liu. 2022. Text2Light: Zero-Shot Text-Driven HDR Panorama Generation. *ACM Trans. Graph.* 41, 6, Article 195 (2022).
- Hyungjin Chung, Jeongsol Kim, Michael T Mccann, Marc L Klasky, and Jong Chul Ye. 2023. Diffusion posterior sampling for general noisy inverse problems. (2023). arXiv:2209.14687 [cs.CV]
- Ugur Cogalan, Mojtaba Bermana, Karol Myszkowski, Hans-Peter Seidel, and Tobias Ritschel. 2022. Learning HDR video reconstruction for dual-exposure sensors with temporally-alternating exposures. *Computers & Graphics* 105 (2022), 57–72.
- Dwip Dalal, Gautam Vashishtha, Prajwal Singh, and Shanmuganathan Raman. 2023. Single image ldr to hdr conversion using conditional diffusion. In *ICIP*. 3533–3537.
- Paul Debevec. 1998. Rendering synthetic objects into real scenes: bridging traditional and image-based graphics with global illumination and high dynamic range photography. In *SIGGRAPH*. 189–198.
- Paul E. Debevec and Jitendra Malik. 1997. Recovering High Dynamic Range Radiance Maps from Photographs. In *Proc. ACM SIGGRAPH*. 369–378.
- Prafulla Dhariwal and Alex Nichol. 2021. Diffusion Models Beat GANs on Image Synthesis. In *NeurIPS*.
- Gabriel Eilertsen, Joel Kronander, Gyorgy Denes, Rafal K. Mantiuk, and Jonas Unger. 2017. HDR image reconstruction from a single exposure using deep CNNs. *ACM Trans. Graph. (Proc. SIGGRAPH)* 36, 6 (2017), 1–15.
- Yuki Endo, Yoshihiro Kanamori, and Jun Mitani. 2017. Deep Reverse Tone Mapping. *ACM Trans. Graph. (Proc. SIGGRAPH Asia)* 36, 6 (2017).
- B. Fei, Z. Lyu, L. Pan, J. Zhang, W. Yang, T. Luo, B. Zhang, and B. Dai. 2023. Generative Diffusion Prior for Unified Image Restoration and Enhancement. In *CVPR*. 9935–9946.
- Param Hanji, Rafal Mantiuk, Gabriel Eilertsen, Saghi Hajisharif, and Jonas Unger. 2022. Comparison of single image HDR reconstruction methods—the caveats of quality assessment. In *Proc. SIGGRAPH*. 1–8.
- Martin Heusel, Hubert Ramsauer, Thomas Unterthiner, Bernhard Nessler, and Sepp Hochreiter. 2017. Gans trained by a two time-scale update rule converge to a local nash equilibrium. *NIPS* 30 (2017).
- Jonathan Ho, Ajay Jain, and Pieter Abbeel. 2020. Denoising diffusion probabilistic models. *NeurIPS* 33 (2020), 6840–6851.
- Xin Huang, Qi Zhang, Ying Feng, Hongdong Li, Xuan Wang, and Qing Wang. 2022. HDR-NeRF: High Dynamic Range Neural Radiance Fields. In *CVPR*. 18398–18408.
- Álvaro Barbero Jiménez. 2023. Mixture of diffusers for scene composition and high resolution image generation. arXiv:2302.02412 [cs.CV]
- So Yeon Jo, Siyeong Lee, Namhyun Ahn, and Suk-Ju Kang. 2021. Deep Arbitrary HDR: Inverse Tone Mapping with Controllable Exposure Changes. *IEEE Trans. Multimedia* (2021).
- Kim Jun-Seong, Kim Yu-Ji, Moon Ye-Bin, and Tae-Hyun Oh. 2022. HDR-Plenoxels: Self-Calibrating High Dynamic Range Radiance Fields. In *ECCV*.
- Nima Khademi Kalantari and Ravi Ramamoorthi. 2017. Deep High Dynamic Range Imaging of Dynamic Scenes. *ACM Trans. Graph. (Proc. SIGGRAPH)* 36, 4 (2017).
- Bahjat Kawar, Michael Elad, Stefano Ermon, and Jiaming Song. 2022. Denoising Diffusion Restoration Models. In *NIPS*.
- Bingxin Ke, Anton Obukhov, Shengyu Huang, Nando Metzger, Rodrigo Caye Daudt, and Konrad Schindler. 2023. Repurposing diffusion-based image generators for monocular depth estimation. (2023). arXiv:2312.02145 [cs.CV]
- Alex Krizhevsky, Ilya Sutskever, and Geoffrey E Hinton. 2012. Imagenet classification with deep convolutional neural networks. *NIPS* 25 (2012).
- Siyeong Lee, Gwon Hwan An, and Suk-Ju Kang. 2018a. Deep chain HDR: Reconstructing a high dynamic range image from a single low dynamic range image. *IEEE Access* 6 (2018), 49913–49924.
- Siyeong Lee, Gwon Hwan An, and Suk-Ju Kang. 2018b. Deep recursive HDR: Inverse tone mapping using generative adversarial networks. In *ECCV*. 596–611.
- Siyeong Lee, So Yeon Jo, Gwon Hwan An, and Suk-Ju Kang. 2020. Learning to generate multi-exposure stacks with cycle consistency for high dynamic range imaging. *IEEE Trans. Multimedia* 23 (2020), 2561–2574.
- Ru Li, Chuan Wang, Jue Wang, Guanghui Liu, Heng-Yu Zhang, Bing Zeng, and Shuaicheng Liu. 2022. UPHDR-GAN: Generative Adversarial Network for High Dynamic Range Imaging With Unpaired Data. *IEEE Trans. Circuits and Systems for Video Technology* 32, 11 (2022), 7532–7546.
- Yu-Lun Liu, Wei-Sheng Lai, Yu-Sheng Chen, Yi-Lung Kao, Ming-Hsuan Yang, Yung-Yu Chuang, and Jia-Bin Huang. 2020. Single-image HDR reconstruction by learning to reverse the camera pipeline. In *CVPR*. 1651–1660.
- Andreas Lugmayr, Martin Danelljan, Andres Romero, Fisher Yu, Radu Timofte, and Luc Van Gool. 2022. RePaint: Inpainting using Denoising Diffusion Probabilistic Models. In *CVPR*.
- Linjie Lyu, Ayush Tewari, Marc Habermann, Shunsuke Saito, Michael Zollhöfer, Thomas Leimkühler, and Christian Theobalt. 2023. Diffusion Posterior Illumination for Ambiguity-Aware Inverse Rendering. *ACM Trans. Graph. (Proc. SIGGRAPH Asia)* 42, 6, Article 233 (2023).
- Rafal Mantiuk, Karol Myszkowski, and Hans-Peter Seidel. 2006. A perceptual framework for contrast processing of high dynamic range images. *ACM Trans. Appl. Percept.* 3, 3 (2006), 286–308.
- Rafal K Mantiuk, Dounia Hammou, and Param Hanji. 2023. HDR-VDP-3: A multi-metric for predicting image differences, quality and contrast distortions in high dynamic range and regular content. arXiv preprint arXiv:2304.13625 (2023).
- Demetris Marnerides, Thomas Bashford-Rogers, Jonathan Hatchett, and Kurt Debattista. 2018. Expandnet: A deep convolutional neural network for high dynamic range expansion from low dynamic range content. In *Comp. Graph. Forum*, Vol. 37. 37–49.
- Ben Mildenhall, Peter Hedman, Ricardo Martin-Brualla, Pratul P Srinivasan, and Jonathan T Barron. 2022. NeRF in the dark: High dynamic range view synthesis from noisy raw images. In *CVPR*. 16190–16199.
- Tomoo Mitsunaga and Shree K. Nayar. 1999. Radiometric self calibration. *CVPR* 1 (1999), 374–380.
- Thomas Müller, Alex Evans, Christoph Schied, and Alexander Keller. 2022. Instant neural graphics primitives with a multiresolution hash encoding. *ACM Trans. Graph. (Proc. SIGGRAPH)* 41, 4 (2022).
- Janne Mustaniemi, Juho Kannala, Jiri Matas, Simo Särkkä, and Janne Heikkilä. 2020. LSD₂-Joint Denoising and Deblurring of Short and Long Exposure Images with Convolutional Neural Networks. In *BMVC*.
- Hironori Nemoto, Pavel Korshunov, Philippe Hanhart, and Touradj Ebrahimi. 2015. Visual attention in LDR and HDR images. In *9th International Workshop on Video Processing and Quality Metrics for Consumer Electronics (VPQM)*.
- Alex Nichol, Prafulla Dhariwal, Aditya Ramesh, Pranav Shyam, Pamela Mishkin, Bob McGrew, Ilya Sutskever, and Mark Chen. 2022. GLIDE: Towards Photorealistic Image Generation and Editing with Text-Guided Diffusion Models. arXiv:2112.10741 [cs.CV]
- Yuzhen Niu, Jianbin Wu, Wenxi Liu, Wenzhong Guo, and Rynson WH Lau. 2021. HDR-GAN: HDR image reconstruction from multi-exposed LDR images with large motions. *IEEE Trans. Image Processing* 30 (2021), 3885–3896.
- Ben Poole, Ajay Jain, Jonathan T Barron, and Ben Mildenhall. 2022. Dreamfusion: Text-to-3d using 2d diffusion. arXiv:2209.14988 [cs.CV]
- Alec Radford, Jong Wook Kim, Chris Hallacy, Aditya Ramesh, Gabriel Goh, Sandhini Agarwal, Girish Sastry, Amanda Askell, Pamela Mishkin, Jack Clark, et al. 2021. Learning transferable visual models from natural language supervision. In *ICML*. 8748–8763.
- Erik Reinhard, Wolfgang Heidrich, Paul Debevec, Sumanta Pattanaik, Greg Ward, and Karol Myszkowski. 2010. *High dynamic range imaging: Acquisition, display, and image-based lighting*. Morgan Kaufmann.
- Mark A Robertson, Sean Borman, and Robert L Stevenson. 2003. Estimation-theoretic approach to dynamic range enhancement using multiple exposures. *J Electronic Imaging* 12, 2 (2003), 219–228.
- Robin Rombach, Andreas Blattmann, Dominik Lorenz, Patrick Esser, and Björn Ommer. 2022. High-Resolution Image Synthesis with Latent Diffusion Models. In *CVPR*.
- Chitwan Saharia, Jonathan Ho, William Chan, Tim Salimans, David J. Fleet, and Mohammad Norouzi. 2023. Image Super-Resolution via Iterative Refinement. *IEEE Trans. Pattern Anal. Mach. Intell.* 45, 4 (2023), 4713–4726.
- Marcel Santana Santos, Tsang Ing Ren, and Nima Khademi Kalantari. 2020. Single Image HDR Reconstruction Using a CNN with Masked Features and Perceptual Loss. *ACM Trans. Graph.* 39, 4, Article 80 (2020), 10 pages.
- Axel Sauer, Katja Schwarz, and Andreas Geiger. 2022. Stylegan-xl: Scaling StyleGAN to large diverse datasets. In *Proc. SIGGRAPH*. 1–10.
- Helge Seetzen, Wolfgang Heidrich, Wolfgang Stuerzlinger, Greg Ward, Lorne Whitehead, Matthew Trentacoste, Abhijeet Ghosh, and Andrejs Vorozcovs. 2004. High dynamic range display systems. *ACM Trans. Graph.* 23, 3 (2004), 760–768.
- Inwook Shim, Joon-Young Lee, and In So Kweon. 2014. Auto-adjusting camera exposure for outdoor robotics using gradient information. In *2014 IEEE/RSJ International Conference on Intelligent Robots and Systems*. 1011–1017.
- Jascha Sohl-Dickstein, Eric Weiss, Niru Maheswaranathan, and Surya Ganguli. 2015. Deep unsupervised learning using nonequilibrium thermodynamics. In *ICML*. PMLR, 2256–2265.
- Yang Song, Jascha Sohl-Dickstein, Diederik P. Kingma, Abhishek Kumar, Stefano Ermon, and Ben Poole. 2021. Score-Based Generative Modeling through Stochastic Differential Equations. In *ICLR*.
- Chao Wang, Ana Serrano, Xingang Pan, Bin Chen, Hans-Peter Seidel, Christian Theobalt, Karol Myszkowski, and Thomas Leimkuehler. 2023a. GlowGAN: Unsupervised Learning of HDR Images from LDR Images in the Wild. (2023).
- Chao Wang, Ana Serrano, Xingang Pan, Krzysztof Wolski, Bin Chen, Hans-Peter Seidel, Christian Theobalt, Karol Myszkowski, and Thomas Leimkühler. 2023b. A Neural

- Implicit Representation for the Image Stack: Depth, All in Focus, and High Dynamic Range. *ACM Trans. Grap.* 42, 6 (2023).
- Lin Wang and Kuk-Jin Yoon. 2022. Deep Learning for HDR Imaging: State-of-the-Art and Future Trends. *IEEE Trans. Pattern Anal. Mach. Intell.* 44 (2022), 8874–8895. Issue 12.
- Yufei Wang, Yi Yu, Wenhan Yang, Lanqing Guo, Lap-Pui Chau, Alex C. Kot, and Bihan Wen. 2023c. ExposureDiffusion: Learning to Expose for Low-light Image Enhancement. In *ICCV*.
- Shangzhe Wu, Jiarui Xu, Yu-Wing Tai, and Chi-Keung Tang. 2018. Deep High Dynamic Range Imaging with Large Foreground Motions. In *ECCV*.
- Qingsen Yan, Dong Gong, Qinfeng Shi, Anton van den Hengel, Chunhua Shen, Ian Reid, and Yanning Zhang. 2019. Attention-guided Network for Ghost-free High Dynamic Range Imaging. In *CVPR*.
- Qingsen Yan, Tao Hu, Yuan Sun, Hao Tang, Yu Zhu, Wei Dong, Luc Van Gool, and Yanning Zhang. 2023. Towards High-quality HDR Deghosting with Conditional Diffusion Models. arXiv:2311.00932 [cs.CV]
- Qingsen Yan, Bo Wang, Peipei Li, Xianjun Li, Ao Zhang, Qinfeng Shi, Zheng You, Yu Zhu, Jinqiu Sun, and Yanning Zhang. 2020. Ghost Removal via Channel Attention in Exposure Fusion. *Computer Vision and Image Understanding* 201 (2020), 103079.
- Ling Yang, Zhilong Zhang, Yang Song, Shenda Hong, Runsheng Xu, Yue Zhao, Wentao Zhang, Bin Cui, and Ming-Hsuan Yang. 2023. Diffusion models: A comprehensive survey of methods and applications. *Comput. Surveys* 56, 4 (2023), 1–39.
- Hanning Yu, Wentao Liu, Chengjiang Long, Bo Dong, Qin Zou, and Chunxia Xiao. 2021. Luminance Attentive Networks for HDR Image and Panorama Reconstruction. In *Comp. Graph. Forum*, Vol. 40. 181–192.
- Lvmin Zhang, Anyi Rao, and Maneesh Agrawala. 2023. Adding conditional control to text-to-image diffusion models. In *ICCV*. 3836–3847.
- Yang Zhang and TO Aydin. 2021. Deep HDR estimation with generative detail reconstruction. In *Comp. Graph. Forum*, Vol. 40. 179–190.

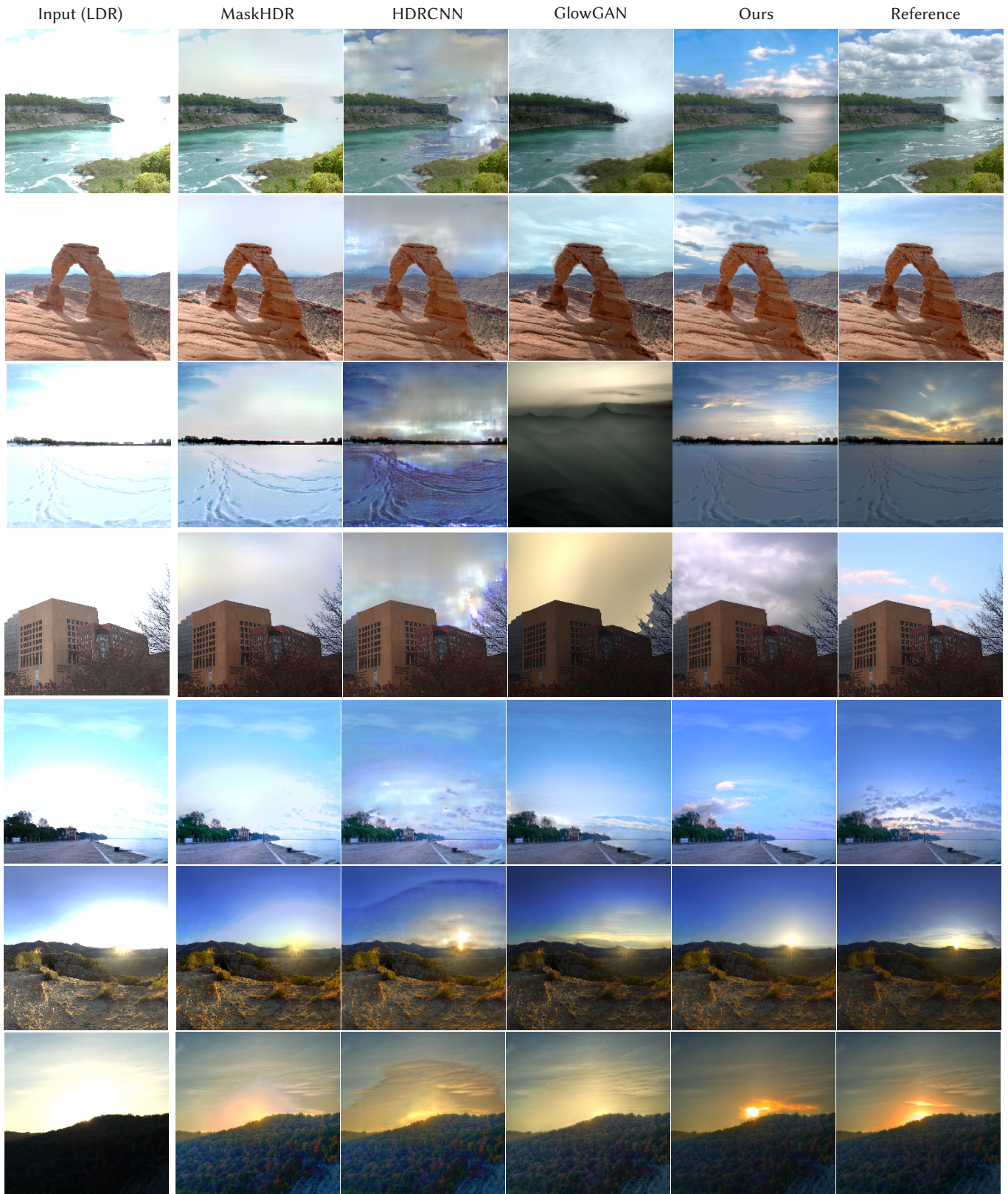


Fig. 11. LDR2HDR reconstruction for our method and competitors given an input LDR images (first column). All HDR images (right columns) are tone-mapped using the same tone-mapper, whose parameters are tuned for each row to achieve the best visual appearance of the corresponding reference HDR image.

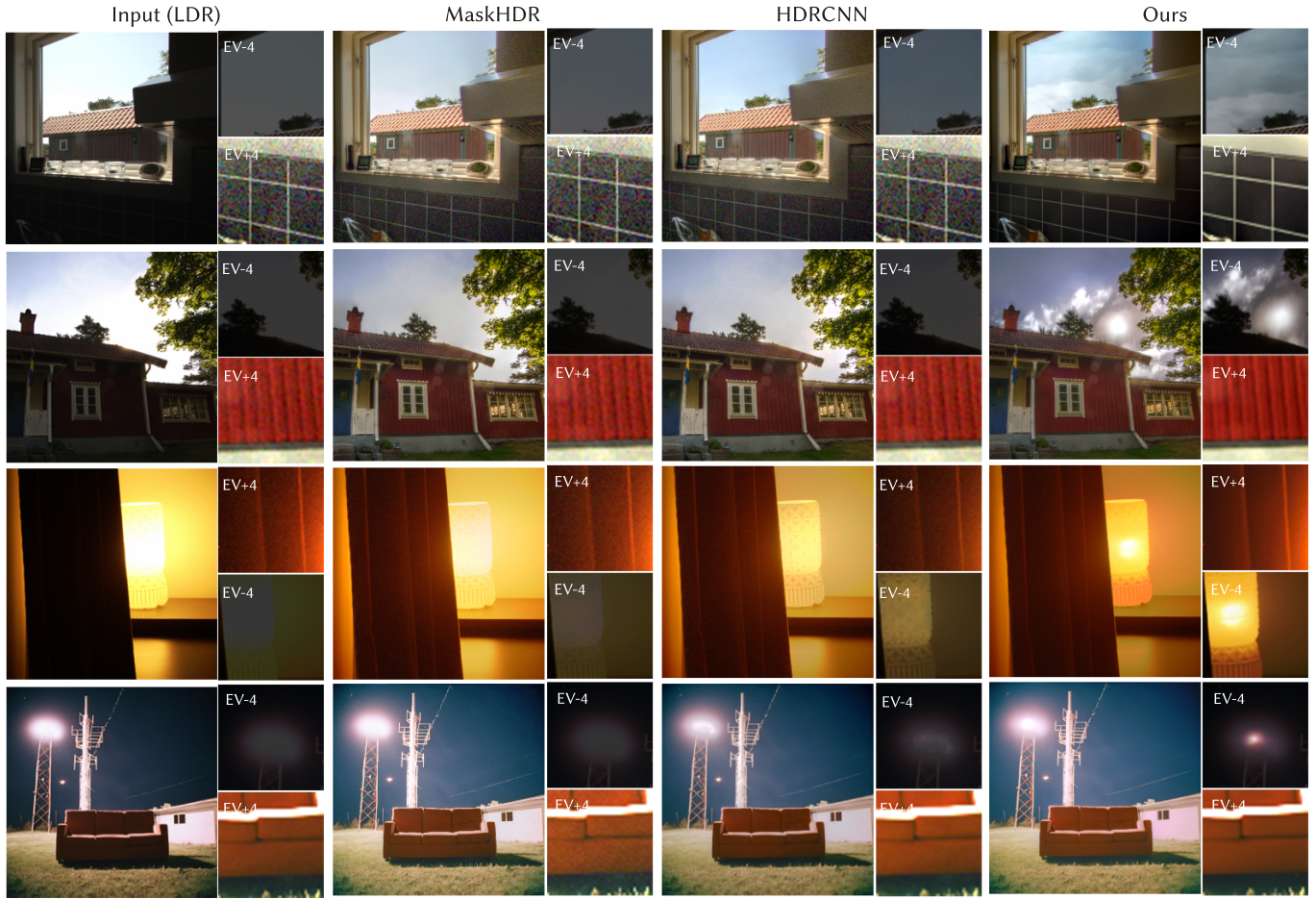


Fig. 12. LDR2HDR reconstruction for MaskHDR, HDRCNN, and Ours methods guided by the input LDR images (left column). Insets show dark, and hence noisy, as well as bright, partially saturated input regions. Other methods can remove some noise, but ours not only gets the semantics right in saturated areas (e.g., for the lamp or sun), but also removes noise in dark areas. The images in the first three rows are examples from the SI-HDR dataset [Hanji et al. 2022], while the image in the last row is an AI-generated image with Stable-Diffusion.